Budgeon
Anthropology

Final Report

Calculations in Support of the Grant
Production of Actinium-225 via High Energy Proton Induced Spallation of Thorium-232

I.C.Gomes Consulting & Investment Inc.

September 21, 2010

PART I – Activation Analysis of the Target

Introduction

Calculations were performed to assess the expected activity of ^{225}Ac and other radioactivity produced in a sample irradiated at a position near the beam stop of the booster beam line at FNAL. This irradiation position was selected based on the accessibility criterion allowing a very simple placement of the sample against the front wall of the beam stop. The beam profile at this position is related to the beam intensity which depends on the number of turns that takes to fill the booster. Despite all beam profiles being already included in the model and calculations performed only the case for 10 turns in the booster is presented in this report. This is made to avoid excessive number of results and also because all profiles are relatively similar with the same total number of protons per second hitting the target.

The case reported is for a thorium target placed in front of the concrete box which encases the steel beam stop. Calculations performed at the FNAL indicated that the beam stop can only take about 20 minutes of the 8 GeV proton beam of the booster beam line at a rate of $6.0x10^{13}$ protons per second before the steel beam stop melts. Considering that the placement of the thorium target will have almost no influence on the power intensity reaching the beam stop, this limitation is expect to be maintained during irradiation. However limitation regarding the activity level in the target for transportation after irradiation is also an important parameter to be taken in consideration. The irradiation scenario selected was to have the target irradiated for a full week, 24 hours per day with a proton intensity of 1.32e+11 protons per second, representing a total number of protons on the target of $8.0x10^{16}$.

General Assumptions

The beam intensity was considered to be $1.32x10^{11}$ protons per second representing $8.0x10^{16}$ protons during the total one week of irradiation. The beam energy is assumed to be 8 GeV. The beam operates at 1 Hz with a pulse length of 1.56 μsec. Considering the nature of the irradiation the calculations where performed in steady state mode, not in pulsed mode because it has no impact on the activation or temperature distribution of the target. The length of irradiation was assumed to be a full week with 24 hours per day irradiation. Based on the hypothesis that the steel beam stop will melt with $6.x10^{13}$ protons per second in 20 minutes results a total number of protons of $7.2x10^{16}$; however it was assumed to be very safe to irradiate the target by roughly the same number of protons but during a much long period of time, namely one week. The assumption of melting the beam stop with $7.2x10^{16}$ protons in 20 minutes is very conservative and it does not consider any heat transfer from the beam stop and surroundings. Then, the irradiation scenario selected is expected to face no problem in being accepted by the safety review committee at FNAL.

Then based on the points outlined above, the full irradiation scenario was assumed to be one week of irradiation at $1.32x10^{11}$ protons per second and a cooling time of 10 days before transporting the irradiated target from the FNAL to Argonne National Laboratory. The geometric configuration of the target was assumed to be a thorium block with external dimensions of 1x2x1 cm^3, being 1-cm thick in the beam direction. The range of an 8GeV proton in a full density thorium is about 5.72m, indicating that only a small amount of the beam energy will be deposited in the thorium target.

In the beam and radiation transport simulations carried out with the MCNPX, the beam stop is also represented in the geometry despite having relatively small influence on the activation results for the target.

Results

Table 1 presents the results for a single Thorium target with dimensions 2cm x 1cm x 1cm placed in front of the entrance of the beam stop inside the concrete block. Table 1 gives, for the irradiation scenario considered the activity (Ci) of the three actinium isotopes of interest (225, 226, and 227) at the end of the irradiation and 10 days after shutdown. The volume of the target is $2cm^3$ and the density of the thorium is 11.67 g/cm^3. As it can be seen, the activity of the ^{225}Ac does reduce by about a factor of 2 during its half-life (10 days) but it is not exactly 50% due to the additional feeding from the decay of ^{225}Ra.

Table 1. Activity (Ci) of the actinium isotopes at the end of the irradiation, 10 and 30 days after shutdown, in a Thorium target with dimensions $2x1x1cm^3$ irradiated during 7 days with 8 GeV protons at a rate of $1.32x10^{11}$ protons/sec.

	After 7 days of Irradiation	10 days after the EOI	30 days after the EOI
^{225}Ac	$3.29x10^{-4}$	$1.88x10^{-4}$	$6.33x10^{-5}$
^{226}Ac	$6.16x10^{-4}$	$1.99x10^{-6}$	$1.32x10^{-9}$
^{227}Ac	$7.09x10^{-7}$	$7.08x10^{-7}$	$7.07x10^{-7}$

Table 2 presents the total gamma ($gamma/cm^3$-sec) in the target geometric configuration and irradiation profile considered. The gamma activity represents the gamma-ray generated informingly distributed inside the sample at just after shutdown, 10, and 30 days after the end of the irradiation. The gamma ray spectrum is given in a multi-group energy structure and the values are the number of gamma-rays generated in the target per cubic centimeter per second within the energy interval of the respective row. As it can be noticed, the high energy gamma-ray component decays much faster than the low energy component what is beneficial in terms of shielding. However, special care should be taken in calculating the dose equivalent for the transportation package because high gamma-rays are still present after 10 or 30 days from the end of irradiation.

Table 2. Estimated multi-group gamma ray activity (γ/cm^3-sec) in target at the time just after, 10, and 30 days after shutdown. Note that the target is $2cm^3$.

Emin	Emax	After 7 days of Irradiation	10 days after the EOI	30 days after the EOI

0.00E+00	1.00E-02	1.61E+09	7.58E+07	2.77E+07
1.00E-02	3.00E-02	1.42E+09	4.74E+07	1.86E+07
3.00E-02	6.00E-02	4.15E+09	2.10E+08	7.99E+07
6.00E-02	1.00E-01	1.09E+09	5.18E+07	2.26E+07
1.00E-01	2.00E-01	1.86E+09	5.84E+07	3.09E+07
2.00E-01	3.00E-01	1.48E+09	2.37E+07	6.38E+06
3.00E-01	5.00E-01	2.15E+09	4.59E+07	1.90E+07
5.00E-01	5.25E-01	1.32E+09	1.42E+07	5.59E+06
5.25E-01	7.50E-01	1.94E+09	4.63E+07	1.12E+07
7.50E-01	1.00E+00	1.76E+09	4.77E+07	1.24E+07
1.00E+00	1.33E+00	1.39E+09	1.81E+07	2.94E+06
1.33E+00	1.66E+00	1.04E+09	1.27E+07	2.78E+06
1.66E+00	2.00E+00	4.29E+08	3.26E+06	1.13E+06
2.00E+00	2.50E+00	4.66E+08	4.57E+06	1.96E+05
2.50E+00	3.00E+00	2.60E+08	1.95E+06	3.25E+05
3.00E+00	4.00E+00	1.74E+08	2.42E+05	2.66E+03
4.00E+00	5.00E+00	4.26E+07	1.18E+01	1.18E+00
5.00E+00	6.00E+00	1.30E+07	3.49E-03	1.80E-03
6.00E+00	7.00E+00	2.73E+06	4.73E-13	4.74E-13
7.00E+00	8.00E+00	6.85E+05	4.45E-14	4.46E-14
8.00E+00	9.00E+00	2.44E+05	9.07E-15	9.07E-15
9.00E+00	1.00E+01	9.45E+04	2.12E-15	2.12E-15
1.00E+01	1.20E+01	6.47E+04	6.23E-16	6.24E-16
1.20E+01	1.70E+01	1.46E+04	1.77E-17	1.77E-17
1.70E+01	3.00E+01	0.00E+00	0.00E+00	0.00E+00
Total		2.26E+10	6.62E+08	2.42E+08

Table 3 presents the fraction of DOE STD-1027-92 CAT-3 threshold for the target considered (a small piece of thorium (2x1x1 cm^3) is irradiated during 7 days with $1.32x10^{11}$ p/s). This table shows how far from the DOE CAT-3 threshold is the hazard of all radioisotopes produced during irradiation at the time that the irradiation ends, 10, and 30 days after shutdown. The results indicate that for the thorium target will be well below the CAT-3 threshold and it would be possible to irradiate the same target during a full week with a beam roughly 700 times more intense than the one used in the simulation and still be below the CAT-3 threshold. This indicates that the experiment will not even be close to pose any serious radiological hazard to the facility. A complete radioisotope inventory is presented in Attachment 4, including both thorium target contribution and copper target holder contribution.

Table 3. Fraction of DOE STD-1027-92 CAT-3 threshold for a $2x1x1cm^3$ irradiated.

	After 7 days of Irradiation	10 days after the EOI	30 days after the EOI
$2x1x1cm^3$	$1.42x10^{-03}$	$5.43x10^{-04}$	$2.11x10^{-04}$

Target			

Table 4 presents the activity of other alpha emitters compared with ^{225}Ac for cooling times of 10 and 30 and days after the end of the irradiation. The activity for all actinium isotopes is basically the activity of ^{225}Ac and for the other alpha emitters are basically the metals thorium, and radium, the alkali metal francium, and the radioactive noble gas radon. The activity of the radon is about twice larger than the actinium 10 days after shutdown and 3 times larger at 20 days after shutdown. All alpha emitters have similar activity and energy; being the overall averaged energy about 6.12MeV.

Table 4. Activity (Ci) of alpha emitters in the irradiated target 10 days after the end of the irradiation.

	Actinium Isotopes	All Alpha Emitters (including Ac)
10 days after EOI	$1.88\text{x}10^{-04}$	$2.29\text{x}10^{-03}$
30 days after EOI	$6.33\text{x}10^{-05}$	$9.89\text{x}10^{-04}$

Conclusions

The irradiation of thorium targets in the booster beam line of the FNAL seems to be highly feasible. The expected activity of ^{225}Ac the target with 2cm x 1cm face area is near 0.2 mCi after 7 days of continuous irradiation with $1.32\text{x}10^{11}$ protons/sec and 10 days of cooling time. These values can be even higher if only the peak of the beam profile is used. The results presented were based on MCNPX/CINDER calculations with validation of the FLUKA code; all results agreed within a 20% range.

The activity calculated indicates that a much more powerful proton beam can be used without making the target to reach the CAT-3 limits. The beam power can be about 700 times higher for the small target $2\text{x}1\text{x}1\text{cm}^3$ without reaching the CAT-3 limits. Previous calculations have indicated that for a better use of the beam time a larger target can be used, allowing a much larger production rate of the ^{225}Ac.

PART II – Activation Analysis of the Surroundings of the Irradiation Position

Abstract

This report has as an objective to assess the activation problem of the thorium target irradiation experiment at FNAL. The results presented are not activation calculation per se, but they provide guidelines to assess any possible impact on the beam stop surroundings due to the irradiation of the target with the low pulse rate 8 GeV proton beam. The average beam intensity is assumed to be 1.32 $x10^{11}$ protons per second and a full week of irradiation is assumed.

1. Introduction

The calculation of the activation for beam stop and surroundings is a quite involving task; it requires the modeling of all materials present around the target and the assessment of the activation during normal operation to compare with the impact caused by placing a target in front of the beam stop tunnel. Considering that the impact is most likely to be minimal, if not negligible, a simple assessment of the beam interaction with the target should suffice for predicting the degree of the potential additional activation caused by placing a thorium target in front of the beam stop structure.

This report presents the calculated flux and current of all significant particles produced in the target by impinging an 8GeV proton beam on one centimeter thick thorium target and the heating produced in the beam stop structure with and without the thorium target.

2. Particle Flux and Current Analysis

The flux of particles in a thin slice near the outer surfaces of the target is an indication of the intensity of the flux leaving the target. Furthermore, the angular distribution of the current of particles across the outer surfaces of the target can provide the number of particles leaving and entering the target or the beam stop tunnel at different directions. In the following sub-sections a number of flux plots are presented for a thin layer at the entrance and exit of the target. Those plots provide an idea of the spatial distribution of the particles while the following tables provide the number and direction of the particles at the outer surfaces of the target and at the entrance of the tunnel. The figures present the particle flux distribution in a layer 0.2cm thick in the direction of the beam and with a cross sectional area of $32cm^2$ (8cmx4cm). The target, which corresponds just the central part of the figures, has a cross sectional area of 2cm by 1cm and a thickness of 1cm. The layer providing the flux estimation for surface of the target facing the incoming beam is placed at a distance of 4cm, in the direction contrary of the beam direction. The layer providing the flux estimation for the back surface of the target is at the end of the target and extending around to cover the cross sectional area indicated previously.

It is also important to note that the current and the angular distribution given in the tables are the total number of particles crossing the indicated surface with the angle

being taken at the point that the particle crosses the surface. The angles are relative to the normal to the surface and the normal of the surfaces points in the direction of the beam. The entrance surface has a cross sectional area of $2cm^2$ (1cm x 2cm) and exit surface of the target has an area of $32cm^2$ (8cm x 4cm) while the surface at the entrance of the tunnel has a surface area of $400cm^2$ (20cm x 20cm). Then, the surface in the back of the target takes into account some of the particles scattered back from the beam stop tunnel. The surface at the entrance of the beam stop tunnel is placed inside the beam stop tunnel at 1mm from the front surface of the concrete structure that houses the steel beam stop. The following analysis is performed for each particle with any significant production in the target.

2.1 Neutrons

Figures 1 and 2 present the neutron flux distribution in a thin slice at the entrance and exit of the target, respectively. As it can be seen, in Figure 2, the neutron flux in the layer on the back of the target is very focused in the central region, indicating a very forward peaked distribution while the neutron flux distribution in Figure 1 is much more spread on the surface and it does not present a very defined beam spot profile as in Figure 2. This indicates that the component of the neutron flux coming back to the room from the beam stop has a very strong presence on the neutron flux spatial distribution in the region represented by the plot.

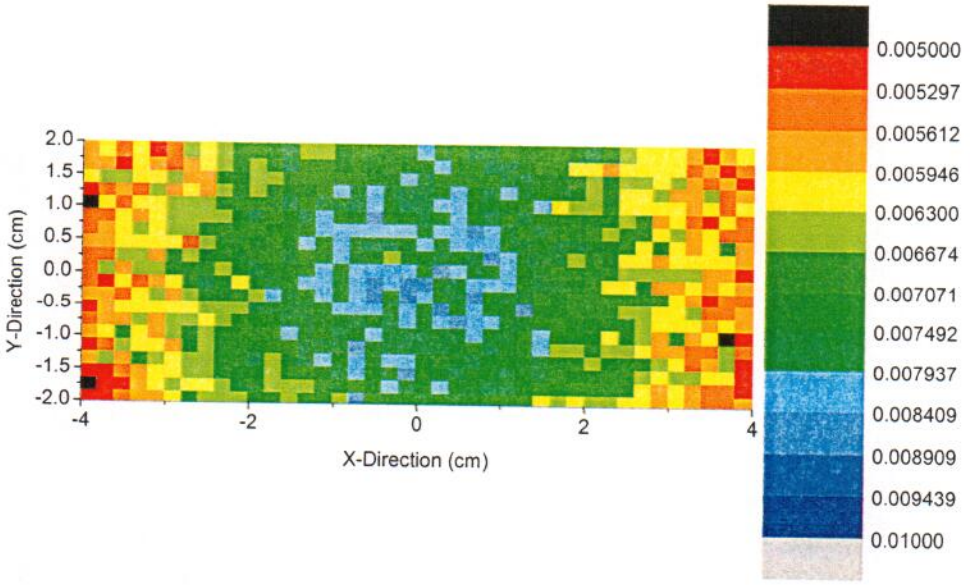

Figure 1. Neutron flux spatial distribution in a layer at the entrance of the target region. The units are neutrons/cm^2-sec normalized for a proton beam intensity of 1.0 proton/sec.

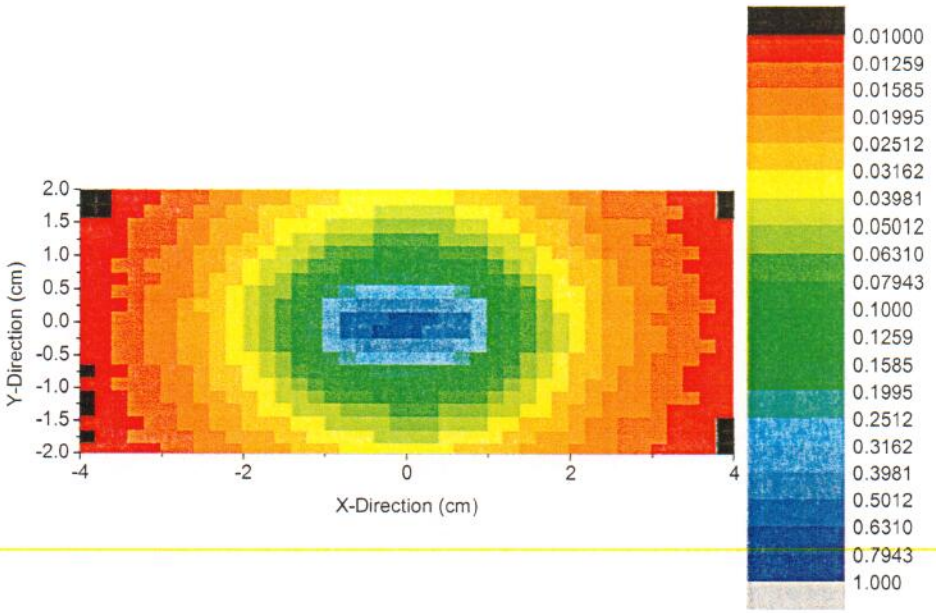

Figure 2. Neutron flux spatial distribution in a layer at the exit of the target region. The units are neutrons/cm^2-sec normalized for a proton beam intensity of 1.0 proton/sec.

Table 1 presents the numeric values of the neutron current through the entrance and exit surfaces of the target and at a surface at the entrance of the beam stop tunnel, for several angular intervals (see a description of the surfaces and angles at the beginning of this section). As it can be seen, with the target present, for each proton that enters the target 0.31 neutrons go into the accelerator hall through the entrance surface of the target, this represents, for a beam intensity of 1.32e+11 protons/ second, 4.09e+10 neutrons/second going into the accelerator hall. Assuming that these neutrons are nearly isotropic this represents a neutron flux of 6.5e+05 n/cm^2-sec at 1 meter from the target and 2.6e+04 n/cm^2-sec at 5 meters from the target. Also in Table 1, one can see that the current coming out of the tunnel when simulating the irradiation scenario without a target is 0.89 neutrons per incident proton beam, indicating a much larger number of neutrons coming out from the tunnel due the beam hitting the walls and steel beam stop inside the tunnel than the ones coming out from the target due the proton beam interaction with the thorium target. It is important to keep in mind that the target front surface has an area of 2cm^2 while the surface at the entrance of the tunnel has an area of 400cm^2. Furthermore, the neutrons coming out of the tunnel with the target has a total number of 0.98 neutrons per proton beam while 0.89 neutrons per proton beam come out of the tunnel without the target present; this indicates that there is only an addition 10% on the number of neutrons coming out of the tunnel when the target is present and 0.31 neutrons per beam proton from the surface of the target, meaning a total maximum additional neutron number of 0.40 neutrons per proton, or less than 50% from the number that goes into the accelerator vault without the target. Then the increase in number of neutrons is small and unlikely to produce any significant activation, beyond the one at normal operation, at all. Based on

that, one can say that the addition of the target, roughly, will increase the number of neutrons in the room by at most 50%. Table 1 also shows that the neutrons going forward are about 0.72 per proton beam and that the large majority will hit positions deep in the beam stop "tunnel" and will not activate the surface of the concrete.

Table 1. Neutron current angular distribution in the entrance, exit surface of the target and entrance of the beam stop tunnel for the cases with and without target material in the target region. The units are number of neutrons per second and normalized for a proton beam intensity of 1.0 proton/sec.

With the Target Present						
Surface	180° to 150°	150° to 120°	120° to 90°	90° to 60°	60° to 30°	30° to 0°
Entrance Target	8.80E-02	1.56E-01	6.63E-02	0.0	0.0	0.0
Exit Target	5.75E-02	1.77E-02	4.52E-03	2.61E-01	3.15E-01	1.47E-01
Tunnel Entrance	6.50E-01	2.24E-01	5.64E-02	3.46E-01	3.15E-01	1.47E-01
Without the Presence of any Target Material						
Entrance Target	3.51E-03	9.58E-04	1.93E-04	0.0	0.0	0.0
Exit Target	5.73E-02	1.59E-02	3.44E-03	0.0	0.0	0.0
Tunnel Entrance	6.44E-01	2.01E-01	4.41E-02	8.15E-05	1.18E-05	1.74E-06

2.2 Protons

Figures 3 and 4 present the proton flux distribution in a thin slice at the entrance and exit of the target, respectively. As it can be seen the proton flux in both layers is very focused in the central region, indicating that the main component of the proton flux is the beam passing through the target and that the region outside the beam spot (a Gaussian distribution with σ_x=1cm and σ_y=0.26cm) has a much weaker flux. The slice that is at the entrance of the beam has a much more focused distribution while on the back of the target, the produced protons from nuclear interactions on the target and scattering of the proton beam produce a wider spatial distribution of the protons.

Table 2 presents the numeric values of the proton current through the entrance and exit surfaces of the target and at a surface at the entrance of the beam stop tunnel for several angular intervals (see a description of the surfaces and angles at the beginning of this section). As it can be seen, for each proton that enters the target 0.0133 protons go into the accelerator hall through the front surface of the target, this represents, for a beam intensity of 1.32e+11 protons/second, 1.74e+09 protons/second going into the accelerator hall. Assuming that these protons are nearly isotropic this represents a proton flux of 2.77e+04 p/cm^2-sec at 1 meter from the target and 1.1e+03 p/cm^2-sec at 5 meters from the target. Also, from the table, one can see that the protons entering the accelerator hall by the surface at the entrance of the beam stop tunnel, when the target is present, is only about 0.00137 protons per proton beam and this value compares with 0.00126 protons

when the there is no thorium target. Based on that comparatively, one can say that there will be an considerable addition of protons directed to the accelerator hall but the absolute number (about 0.0134 proton per proton beam) of this addition is much smaller than the neutron flux into the accelerator hall as such resulting in a much less activation than the neutron activation.

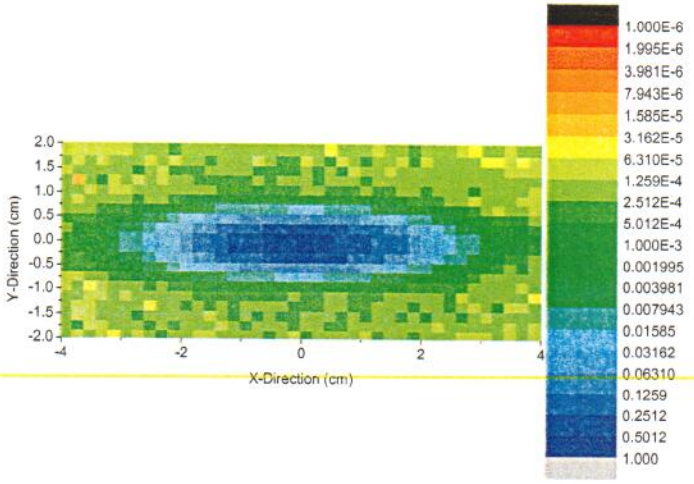

Figure 3. Proton flux spatial distribution in a layer at the entrance of the target region. The units are protons/cm^2-sec normalized for a proton beam intensity of 1.0 proton/sec.

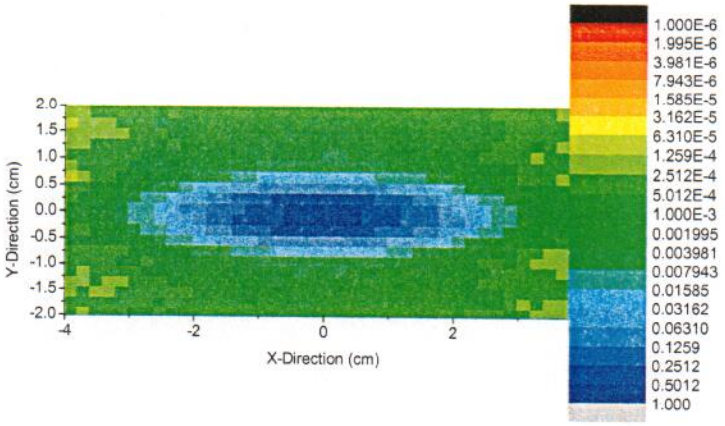

Figure 4. Proton flux spatial distribution in a layer at the entrance of the target region. The units are protons/cm^2-sec normalized for a proton beam intensity of 1.0 proton/sec.

Table 2 also shows that the protons hitting the target are only 65% of the total beam, which is consistent with the Gaussian distribution of the beam profile with a standard deviation of 1cm in the x-direction and 0.26cm in the y-direction. Table 2 indicates that basically all protons from the beam go to the beam stop tunnel plus a small

fraction created by target multiplication of protons. The very large majority of the protons will be in the very forward direction as such they will hit positions deep inside the beam stop "tunnel" and will not activate the surface of the concrete.

Table 2. Proton current angular distribution in the entrance, exit surface of the target and entrance of the beam stop tunnel for the cases with and without target material in the target region. The units are number of protons per second and normalized for a proton beam intensity of 1.0 proton/sec.

With the Target Present						
Surface	180° to 150°	150° to 120°	120° to 90°	90° to 60°	60° to 30°	30° to 0°
Entrance Target	3.59E-03	6.65E-03	3.04E-03	0.0	0.0	6.53E-01
Exit Target	1.01E-04	5.50E-06	3.00E-06	1.21E-02	2.45E-02	1.02E+00
Tunnel Entrance	1.25E-03	9.54E-05	2.65E-05	1.57E-02	2.45E-02	1.02E+00
Without the Presence of any Target Material						
Entrance Target	3.50E-06	5.00E-07	0.0	0.0	0.0	6.53E-01
Exit Target	1.00E-04	4.00E-06	1.00E-06	0.0	0.0	1.00E-01
Tunnel Entrance	1.20E-03	5.55E-05	7.00E-06	0.0	0.0	1.00E+00

2.3 Deuterons

Figures 5 and 6 present the deuteron flux distribution in a thin slice at the entrance and exit of the target, respectively. As it can be seen the deuteron flux in the layer on the back of the target is much focused in the central region, indicating a very forward peaked distribution, while in the backward direction is much diffused with a much lower intensity.

Table 3 presents the numeric values of the deuterons current through the entrance and exit surfaces of the target and at a surface at the entrance of the beam stop tunnel for several angular intervals (see a description of the surfaces and angles at the beginning of this section). As it can be seen, for each proton that enters the target 4.8e-04 deuterons go into the accelerator hall, this represents, for a beam intensity of 1.32e+11 protons/second, 5.7e+07 deuterons/second going into the accelerator hall. Assuming that these deuterons are nearly isotropic this represents a deuteron flux of 9.11e+02 d/cm^2-sec at 1 meter from the target and 3.65e+01 d/cm^2-sec at 5 meters from the target. Also, from the table, one can see that the deuterons entering the accelerator hall by the surface at the entrance of the beam stop tunnel, when the target is present, is only about 4.6e-05 deuterons per proton beam and this value compares with 4.85e-05 deuterons when the there is no thorium target (Note that the results without the target is bigger than with the target, indicating that the statistical uncertainty is larger than the difference of having the target or not). Based on that comparatively, one can say that there will be a considerable addition of deuterons directed to the accelerator hall but the absolute number (about 4.8e-04 deuteron per proton beam) of this addition is much smaller than the neutron flux into the accelerator hall as such resulting in a near negligible activation.

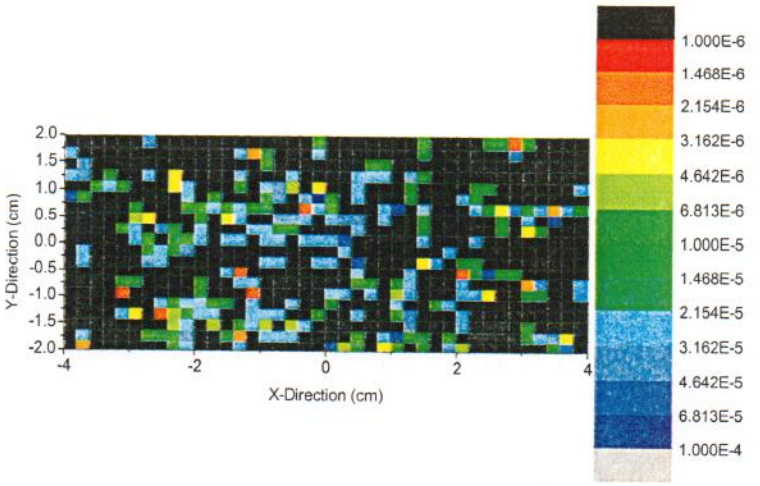

Figure 5. Deuteron flux spatial distribution in a layer at the entrance of the target region. The units are deuterons/cm^2-sec normalized for a proton beam intensity of 1.0 proton/sec.

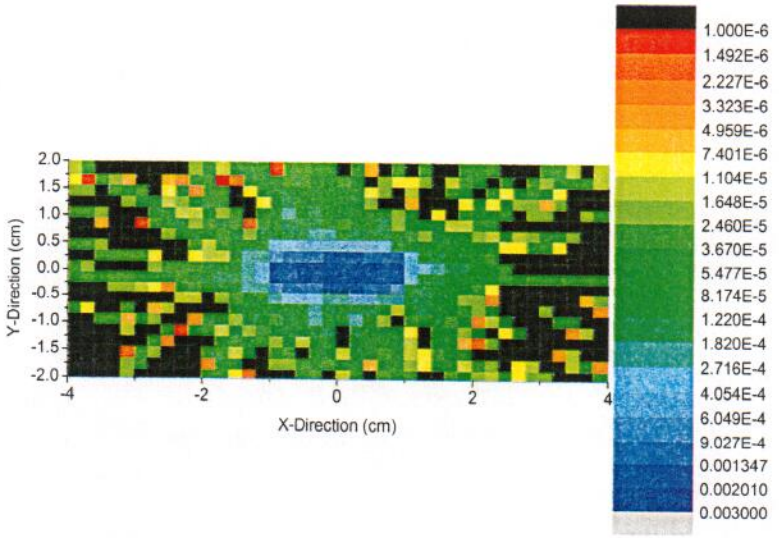

Figure 6. Deuteron flux spatial distribution in a layer at the exit of the target region. The units are deuterons/cm^2-sec normalized for a proton beam intensity of 1.0 proton/sec.

Table 3. Deuteron current angular distribution in the entrance, exit surface of the target and entrance of the beam stop tunnel for the cases with and without target material in the target region. The units are number of deuterons per second and normalized for a proton beam intensity of 1.0 proton/sec.

With the Target Present						
Surface	180° to 150°	150° to 120°	120° to 90°	90° to 60°	60° to 30°	30° to 0°

Entrance Target	1.05E-04	2.13E-04	1.16E-04	0.0	0.0	0.0
Exit Target	3.50E-06	2.00E-06	5.00e-07	3.91E-04	6.38E-04	3.04E-04
Tunnel Entrance	3.05E-05	1.20E-05	3.50E-06	4.60E-04	6.38E-04	3.05E-04
Without the Presence of any Target Material						
Entrance Target	0.0	0.0	0.0	0.0	0.0	0.0
Exit Target	3.00E-06	5.00E-07	5.00E-07	0.0	0.0	0.0
Tunnel Entrance	3.55E-05	1.15E-05	1.50E-06	0.0	0.0	0.0

2.4 Pions

Figures 7 and 8 present the pion_+ flux distribution in a thin slice at the entrance and exit of the target, respectively. As it can be seen the pion_+ flux in the layer on the back of the target is much focused in the central region, indicating a very forward peaked distribution, while in the backward direction is much diffused with a much lower intensity.

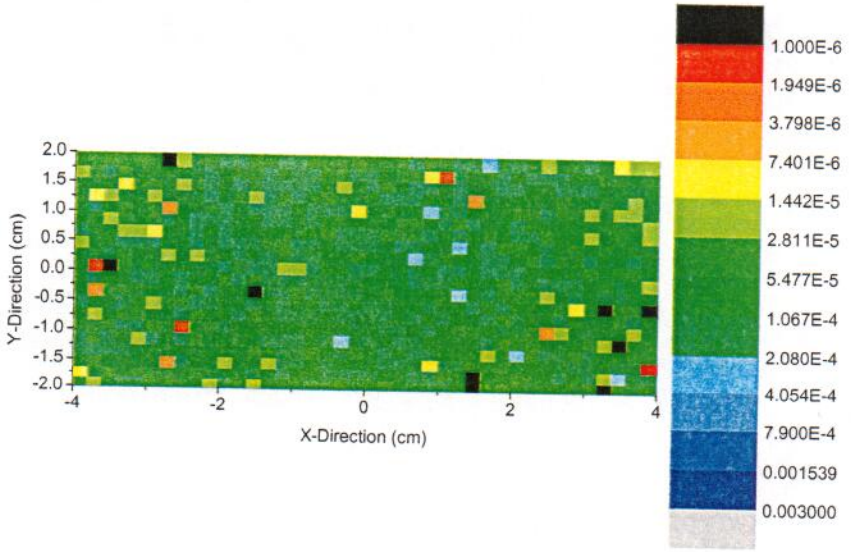

Figure 7. Pion_+ flux spatial distribution in a layer at the entrance of the target region. The units are pions/cm^2-sec normalized for a proton beam intensity of 1.0 proton/sec.

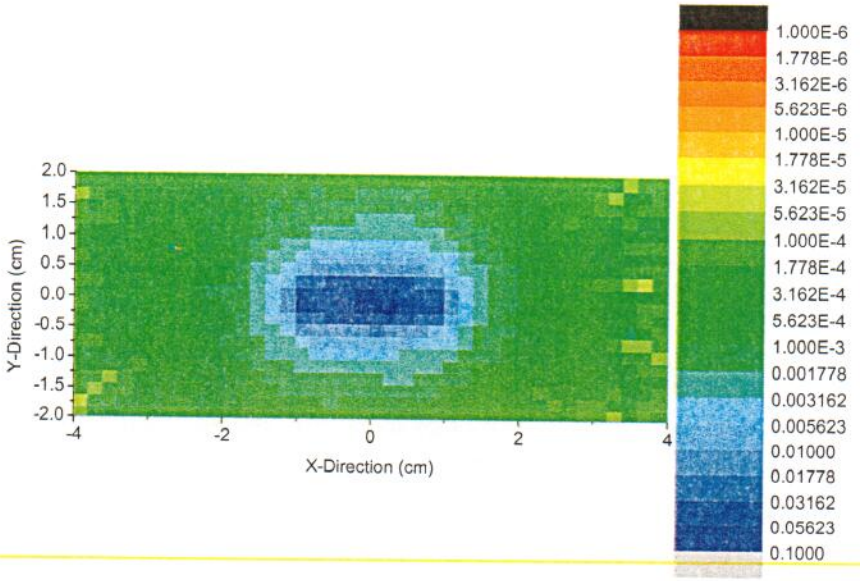

Figure 8. Pion_+ flux spatial distribution in a layer at the exit of the target region. The units are pions/cm^2-sec normalized for a proton beam intensity of 1.0 proton/sec.

Table 4 presents the numeric values of the pions_+ current through the entrance and exit surfaces of the target and at a surface at the entrance of the beam stop tunnel for several angular intervals (see a description of the surfaces and angles at the beginning of this section). As it can be seen, for each proton that enters the target 5.6e-03 pions_+ go into the accelerator hall, this represents, for a beam intensity of 1.32e+11 protons/ second, 7.4e+08 pions/second going into the accelerator hall. Assuming that these pions are nearly isotropic this represents a pion flux of 1.17e+04 pion/cm^2-sec at 1 meter from the target and 4.7e+02 pion/cm^2-sec at 5 meters from the target. Also, from the table, one can see that the pions_+ entering the accelerator hall through the surface at the entrance of the beam stop tunnel, when the target is present, is only about 2.91e-03 pions_+ per proton beam and this value compares with 2.79e-03 pions_+ when the there is no thorium target. Table 4 also shows that the pions going forward are about 7.9e-02 per proton beam and that the large majority will hit positions deep in the beam stop "tunnel" and will not activate the surface of the concrete. Based on that, one can say that there will be a small addition of pions_+ directed to the accelerator hall but the absolute number (about 5.6e-03 pions_+ per proton beam) of this addition is much smaller than the neutron flux into the accelerator hall as such resulting in a small additional activation.

Table 4. Pion current angular distribution in the entrance, exit surface of the target and entrance of the beam stop tunnel for the cases with and without target material in the target region. The units are number of pions per second and normalized for a proton beam intensity of 1.0 proton/sec.

With the Target Present						
Surface	180° to	150° to	120° to	90° to	60° to	30° to 0°

	150°	120°	90°	60°	30°	
Entrance Target	1.52E-03	2.78E-03	1.23E-03	0.0	0.0	0.0
Exit Target	2.55E-04	1.25E-05	4.50E-06	7.64E-03	2.39E-02	4.73E-02
Tunnel Entrance	2.72E-03	1.41E-04	5.20E-05	9.73E-03	2.39E-02	4.73E-02
Without the Presence of any Target Material						
Entrance Target	1.40e-05	0.0	0.0	0.0	0.0	0.0
Exit Target	2.40E-04	3.50E-06	5.00E-07	0.0	0.0	0.0
Tunnel Entrance	2.74E-03	3.70E-05	8.00E-06	0.0	0.0	0.0

2.5 Alphas

Figures 9 and 10 present the alpha flux distribution in a thin slice at the entrance and exit of the target, respectively. As it can be seen the alpha flux in the layer on the back of the target is much focused in the central region, indicating a very forward peaked distribution, while in the backward direction is much diffused with a much lower intensity.

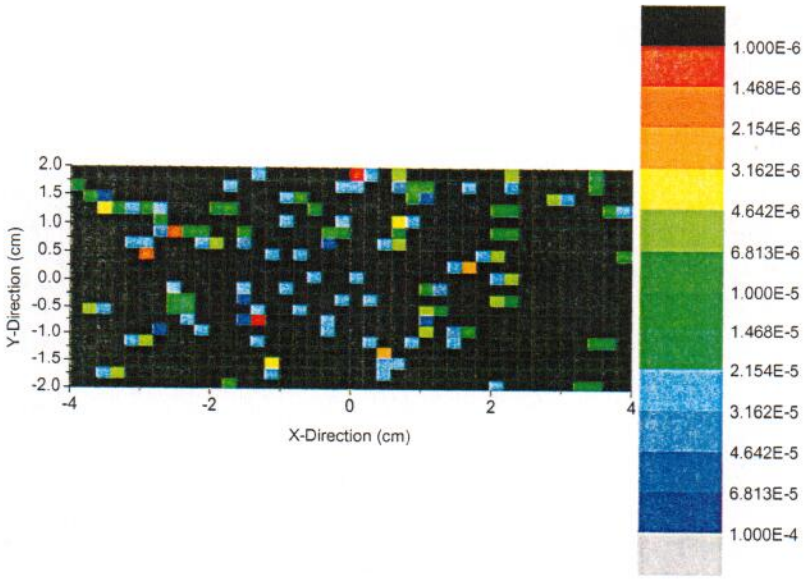

Figure 9. Alpha flux spatial distribution in a layer at the entrance of the target region. The units are alphas/cm^2-sec normalized for a proton beam intensity of 1.0 proton/sec.

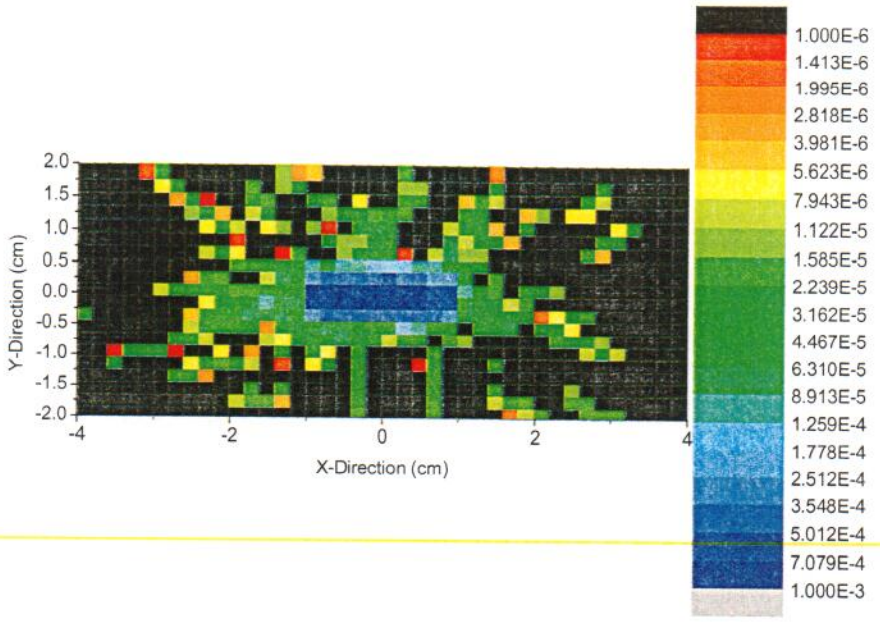

Figure 10. Alpha flux spatial distribution in a layer at the exit of the target region. The units are alphas/cm^2-sec normalized for a proton beam intensity of 1.0 proton/sec.

Table 5 presents the numeric values of the alphas current through the entrance and exit surfaces of the target and at a surface at the entrance of the beam stop tunnel for several angular intervals (see a description of the surfaces and angles at the beginning of this section). As it can be seen, for each proton that enters the target 2.1e-04 alphas go into the accelerator hall, this represents, for a beam intensity of 1.32e+11 protons/ second, 2.77e+07 alphas/second going into the accelerator hall. Assuming that these alphas are nearly isotropic this represents an alpha flux of 4.41e+02 alphas/cm^2-sec at 1 meter from the target and 17.6 alphas/cm^2-sec at 5 meters from the target. Also, from the table, one can see that the alphas entering the accelerator hall through the surface at the entrance of the beam stop tunnel, when the target is present, is only about 3.41e-06 alphas per proton beam and this value compares with 2.91e-06 alphas when the there is no thorium target. Table 4 also shows that the alphas going forward are about 3.99e-04 alphas per proton beam and that the large majority will hit positions deep in the beam stop "tunnel" and will not activate the surface of the concrete. Based on that, one can say that there will be a small addition of alphas directed to the accelerator hall but the absolute number (about 2.1e-04 alphas per proton beam) of this addition is much smaller than the neutron flux into the accelerator hall as such resulting in a small additional activation.

Table 5. Alpha current angular distribution in the entrance, exit surface of the target and entrance of the beam stop tunnel for the cases with and without target material in the target region. The units are number of alphas per second and normalized for a proton beam intensity of 1.0 proton/sec.

With the Target Present						
Surface	180° to 150°	150° to 120°	120° to 90°	90° to 60°	60° to 30°	30° to 0°
Entrance Target	5.60E-05	9.50E-05	4.90E-05	0.0	0.0	0.0
Exit Target	5.00E-07	5.00E-07	0.0	1.20E-04	1.88E-04	9.10E-05
Tunnel Entrance	2.41E-06	1.00E-06	0.0	1.41E-04	1.88E-04	9.10E-05
Without the Presence of any Target Material						
Entrance Target	0.0	0.0	0.0	0.0	0.0	0.0
Exit Target	0.0	5.00E-07	0.0	0.0	0.0	0.0
Tunnel Entrance	1.41E-06	1.5e-06	0.0	0.0	0.0	0.0

3. Heating

The beam stop structure and surroundings will receive heat deposited by beam particles and all types of particles emanating from the beam stop and target. Figure 11 displays the spatial heating distribution on a horizontal plane leveled with the beam centerline. The unit of the heating plotted is MeV/gram per proton beam. The incident energy of the proton beam is 8GeV; then the total energy available in the beam for the intensity of 1.32e+11 protons/second is 168 Watts. The calculated energy deposited in the target is 1.0 Watt and in the steel beam stop is 125.6 Watts, indicating the steel beam stop is the largest radiation producing element of the irradiation set-up what justifies its dominance in the activation of the accelerator hall through neutrons that stream through the beam stop tunnel.

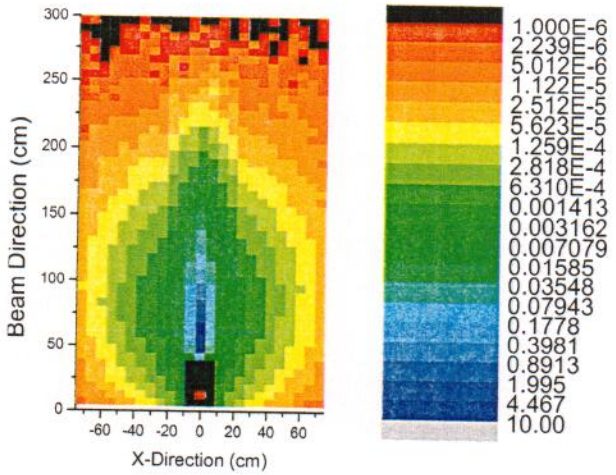

Figure 11. Total heating deposition on the horizontal plane leveled with the beam centerline. The unit is MeV/gram per proton beam.

Conclusions

Based on the analysis performed, the conclusion is that the major and principal contributor for the activation of the accelerator hall is neutrons scattered back from the steel beam stop. The neutrons produced in the target in the backward direction will increase the neutron population, during irradiation, in the accelerator hall by roughly 50% what should not be a major impact in terms of activation of the accelerator hall. Furthermore, the irradiation campaign proposed will have 1.32e+11 protons/second during 1 week; then representing a total number of protons 8.0e+16 protons for the whole campaign. The MI-8 absorber can take 6.8e+18 protons per year, based on FNAL guidelines, which represents the ADESH limit due to ground water contamination. Then, this irradiation will take about 1.17% of the full year limit and even if fully charged for the additional 50% of neutrons in the accelerator hall due to the presence of the thorium target it would represent 1.76% of the year limit of the MI-8 absorber. However, the additional neutrons in the accelerator hall are mainly low energy neutrons when compared with the neutrons produced in the beam stop or in the forward direction at the target. This is due to the fact that the neutrons going into the accelerator hall are mainly produced in the backward direction and the momentum balance at the collision site, where they are produced, predicts a very low energy for such neutrons when compared with the forward ones. Then, as a conclusion those neutrons should not have a significant contribution for the ground water activation. Regarding the forward peaked component of the neutron and other particles production at the target, they will be more than one hundred times lower than the ones produced in the steel beam stop (based on the heat deposition on the target and on the steel beam stop), and as such should not add much to the ground water activation.

Regarding the other particles produced in the thorium target, the calculations estimate that none will have a significant impact on the activation of materials present in the accelerator hall.

Finally, it is safe to say that the irradiation of the thorium target will not add significant activation to the MI-8 absorber structure and surroundings.

PART III – Heating Issues

Introduction

The same assumptions as the previous sections was adopted for this set of calculation, namely, 1.32×10^{11} p/s, 8GeV protons, 2x1x1 cm^3 thorium full density target.

General Assumptions

The sample is irradiated for the full time during one week with an average beam intensity of 1.32×10^{11} protons/second and processed 10 days after irradiation ends.

The geometry configuration used to simulate the thorium target was a block with external dimensions of 2x1x1 cm^3.

The third dimension of the block is the direction of the beam; then the beam crosses, in the model, 1cm of thorium target. The range of an 8GeV proton in thorium is about 5.72m, indicating that only a very small amount of the beam energy will be deposited in the thorium target.

The beam stop is represented in the geometry despite having relatively small influence on the results, increasing computer time, and worsening statistics but it was used anyway in the MCNPX simulations because the code can handle this type of calculation easily.

Results

The transport calculation was performed with the MCNPX code. The FLUKA code was also used to validate the results; several cases were run and the MCNPX/CINDER results compared with the FLUKA results. The comparison of the results was presented in the Preliminary Report I.

The calculated heating deposition due the interaction of the beam and all secondaries particles produced by the beam interaction with the target is calculated to be 1.0 watt. It is assumed that the target will have no other form of heat transfer but radiation. This is a conservative approach because the air convection around the sample is another heat transfer mechanism that is relevant beside conduction to the target holder and even enlargement of the radiation heat transfer area that the target holder may represent. To calculate the operating temperature to remove the calculated heating by radiation the following formula is used:

$$R = P/A = \varepsilon \sigma [(T_1)^4-(T_2)^4] \quad (1)$$

Where:

R is the emitted heating by radiation; P is the power emitted; A is the area of the free surface for radiation heat transfer; ε is the emissivity of the material; σ is the Stefan-Boltzmann constant ($\sigma=5.67 \times 10^{-8}$ $W/[m^2.K^4]$); T_1 is the temperature of the material; and T_2 is the temperature of the environment.

In the thorium target irradiated at the booster line of the FNAL, the variables of equation (1) have the following values:

$P = 1.0W$

$A = 1.x10^{-3}$ (the target has 4 surfaces with $2cm^2$ and 2 with $1cm^2$).

ε is for thorium between 0.35 and 0.4[1]

T_2 is assumed 300°K

T_1 is the unknown.

Then solving for T_1, we have:

$1.0/1.x10^{-3} = 0.35 * 5.67x10^{-8} * [(T_1)^4 - 8.1x10^9];$

Then;

$T_1 = [1.79x10^{11}+8.1x10^9]^{0.25} = 491.78°K$

This indicates that the stead state temperature of the target to radiate 1.0W is ~219°C while the melting temperature of the thorium is 1750°C. This calculated temperature is only for radiation heat transfer and it is an upper limit that will be reduced by free air convection and other potential heat transfer mechanisms to/by the sample holder. This temperature is showing that there is plenty of room to operate the target before it reaches near the melting point. Situations such as the beam collapsing to a small spot would not be enough to melt the target if corrective action is taken in seconds/minutes time, as shown below. Also, it is important to point out that the target can be covered with a thin foil of a metal with higher emissivity, or painted with carbon (AquaDag) what would reduce the operating temperature of the target (by example, an emissivity of 0.9 would result in an operating temperature of 407°K). In any case, the temperature of the target is going to be low enough to prevent a high release rate of the radioactivity generated in the target, what is of importance to minimize the impact of the experiment on adding radioactivity to the irradiation position.

Another point if the pulse structure of the beam can have an important influence on the temperature. A simple way to check this is to calculate the time that will take to the target to hit the operating temperature and the temperature that the target had to rise to assimilate one pulse. The heat capacity of the thorium metal is equated as:

$C_p=24.905 + 4.049x10^{-3} T + 5.591x10^{-6} T^2$ J/mol.K[2]

To find the time that 1.0W would bring a $2cm^3$ thorium block from 300°K to 491.59°K we use:

$Q = m C_p \Delta T = (23/232.0381) * 28.14 * 192. = 610.85$ J

Where:

m = number of moles, the mass of the target is 23g, 1 mol is 232.0381

C_p is given above and assessed at 480°K

$\Delta T = (491.78 - 300)°K$

---

[1] Use of Energy, Minerals and Changing Techniques by Kaulir Kisor Chatterjee

[2] Heat Capacity of Well-Characterized Thorium Metal from 298°K to 700°K; Franklin L. Oetting and David T. Peterson

To calculate the time, we use:

$t = Q/P = 610.85 / 1.0 = 610.85$ sec. = 10.18 minutes.

This is the lowest time because it does not account for any heat transfer and all the energy is used to increase the target temperature. The result indicates that the target will reach operating temperature (~492°K) in more than 10 minutes.

Now, the temperature increase in one pulse would be:

$1.0 = (23/232.0381) * 28.14 * \Delta T \Rightarrow \Delta T = 0.36$ °K

This indicates that the ramp up of the temperature is slow.

Another topic of importance is the level of radiation stored in the target. Table 1 presents the fraction of DOE STD-1027-92 CAT-3 threshold after one week of irradiation of the thorium (2x1x1 cm^3) target. This table shows how far from the DOE CAT-3 threshold is the hazard of the collective radioisotopes produced during irradiation at the time that vault is open. The results indicate that the CAT-3 fraction is very small and that there is plenty of room to have a much higher beam power and still having only to follow CAT-3 safety guidelines to transport and process the target. Attachment 4 contains a listing of radioisotopes attributed to the target, aluminum target stand, and copper target holder with their individual fraction of the CAT-3 limit.

Table 1. Fraction of DOE STD-1027-92 CAT-3 threshold for a 2x1x1cm^3 irradiated.

	After 7 days of Irradiation	10 days after the EOI	30 days after the EOI
2x1x1cm^3 Target	$1.43x10^{-03}$	$5.43x10^{-04}$	$2.11x10^{-04}$

Conclusions

The irradiation of thorium targets in the booster beam line of the FNAL seems to be highly feasible. The results presented were based on MCNPX/CINDER calculations with validation of the FLUKA code and results agreed within a 20% range.

The operating temperature of the target is expected to be 219°C during the irradiation not causing any problem of melting the target.

The activity calculated indicates that a much more powerful proton beam can be used without making the target to reach the CAT-3 limits. The beam power can be about 700 times higher for the small target 2x1x1cm^3 without reaching the CAT-3 limits, what represents a promising future for this production technique.

Attachment 4

Radioisotope Inventory as a Fraction of DOT CAT 3 Limits[3]

[3] LA-12981-MS, "Table of DOE-STD-1027-92 Hazard Category 3", Threshold Quantities for ICRP-30 List of 757 Radionuclides" August 1995

Radioisotopes attributed to the Cu[5] target holder at shutdown and 10 days post EOI:

	EOI	10 days
24Na	8.61E-07	1.43E-11
28Mg	9.01E-08	3.12E-11
42K	5.05E-08	7.21E-14
43K	1.29E-07	7.45E-11
43Sc	5.12E-09	7.85E-28
44Sc	1.17E-07	1.80E-26
44mSc	1.90E-07	1.11E-08
46Sc	7.48E-08	6.88E-08
47Sc	2.08E-08	2.74E-09
48Sc	1.65E-07	3.66E-09
48V	4.13E-07	2.68E-07
48Cr	9.70E-09	7.10E-12
51Cr	1.01E-08	7.88E-09
52Mn	7.59E-07	2.20E-07
54Mn	1.80E-08	1.76E-08
56Mn	8.38E-08	3.60E-35
52Fe	1.23E-08	1.72E-17
59Fe	1.62E-08	1.39E-08
55Co	5.88E-08	4.42E-12
56Co	1.49E-07	1.36E-07
57Co	4.02E-09	3.92E-09
58Co	1.33E-07	1.21E-07
60Co	7.00E-09	6.98E-09
56Ni	1.19E-08	3.83E-09
57Ni	7.51E-08	7.40E-10

[5] P. Kozma and J. Kliman, SPALLATION OF COPPER BY 9 GeV/c PROTONS AND DEUTERONS, Czech. J. Phys. B 38 (1988)